Green Chemistry

PAPER

View Article Online
View Journal

Cite this: DOI: 10.1039/d2gc03744k

High density cellulose nanofibril assembly leads to upgraded enzymatic and chemical catalysis of fermentable sugars, cellulose nanocrystals and cellulase production by precisely engineering cellulose synthase complexes†

Ran Zhang, ‡[a,b,c] Zhen Hu,‡[a,b,d] Hao Peng,[a,b] Peng Liu,[a,b] Youmei Wang,[a,b] Jingyang Li,[b,e] Jun Lu,[c] Yanting Wang, [a,b,c] Tao Xia*[b,c,f] and Liangcai Peng*[a,b,c]

Although cellulose represents the most abundant biomass resource on Earth, its natural recalcitrance hinders its application for low-cost biofuels and high-value bioproducts on a large scale. In this study, we generated less recalcitrant cellulose nanofibril substrates by site-specific mutations and knockouts of three OsCESA4,7,9 isoforms that are essential as cellulose synthase complexes for the cellulose biosynthesis of secondary cell walls in rice. As a comparison with the wild type form, three genetically-engineered CESAs isoforms independently generated cellulose nanofibrils with the average lengths reduced by 63%, which accounts for the high density of the amorphous cellulose chains as the initial breakpoints for the consistently enhanced biomass enzymatic hydrolysis into fermentable sugars. The genetically modified cellulose nanofibrils efficiently produce ideal nanocrystals with the most reduced dimension to-date in three knockout lines, which are applicable as optimal intermediates for highly valuable bioproducts. The improved cellulose nanofibrils are also effective in inducing the secretion of lignocellulose-degradation enzymes from fungi (*T. reesei*) with the two cellulase (exoglucanases, β-glucosidases) activities elevated by 100% and 138%, and the total protein level increased by 44%. Our data thus reveal a novel green strategy for achieving high-quality diverse bioproduction by integrating the precise genetic modification of lignocellulose substrates with efficient biomass process technology.

Received 6th October 2022,
Accepted 4th January 2023

DOI: 10.1039/d2gc03744k

rsc.li/greenchem

1. Introduction

Plant cell walls provide most of the terrestrial biomass resources that are sustainable for the manufacturing of biofuels and bioproducts.[1–3] As a major component of plant cell walls and a large carbon sink from plant photosynthesis, cellulose is composed of β-1,4-glucan chains that are aligned to form crystalline microfibrils by hydrogen bonds and other intermolecular forces.[4,5] The crystalline structure of cellulose microfibrils influences biological processes that control plant growth and mechanical strength, and it also determines lignocellulose recalcitrance against chemical and enzymatic diges-

[a]*Key Laboratory of Fermentation Engineering, National "111" Center for Cellular Regulation & Molecular Pharmaceutics, Cooperative Innovation Center of Industrial Fermentation, Hubei Key Laboratory of Industrial Microbiology, Hubei University of Technology, Wuhan, 430068, China. E-mail: lpeng@mail.hzau.edu.cn, 121412336@qq.com, huzhen19900817@163.com, 545522097@qq.com, 752624417@qq.com, wym_quiet@yeah.net, wyt@mail.hzau.edu.cn*

[b]*Biomass and Bioenergy Research Centre, College of Plant Science & Technology, Huazhong Agricultural University, Wuhan 430070, China. E-mail: xiatao@mail.hzau.edu.cn, jingyanglee@163.com*

[c]*Laboratory of Biomass Engineering & Nanomaterial Application in Automobiles, College of Food Science & Chemical Engineering, Hubei University of Arts & Science, Xiangyang 441003, China. E-mail: xflujun@163.com*

[d]*College of Resources & Environment, Huazhong Agricultural University, Wuhan, 430070, China*

[e]*Haikou Experimental Station, Chinese Academy of Tropical Agricultural Sciences, Haikou 570102, China*

[f]*College of Life Science & Technology, Huazhong Agricultural University, Wuhan, 430070, China*

† Electronic supplementary information (ESI) available: Fig. S1. Phenotypes and genetic information of the site-mutants and knockout lines of OsCESA4,7,9 isoforms. Fig. S2. The ratio of arabinose to xylose of the non-KOH-extractable hemicelluloses of the site-mutants and knockout lines of OsCESA4,7,9 isoforms. Table S1. Primers used for CRISPR-Cas9 editing of the OsCESA4, 7, 9 isoforms. Table S2. Primers used for the detection of the off-target mutagenesis in *CESA*-edited plants. Table S3. LC-MS/MS identification of *T. reesei*-secreted enzymes after incubation with nanofibril substrate. Table S4. Correlation analyses of the major wall parameters by representative site-mutants and knockout lines and Spearman's method (n = 8). See DOI: https://doi.org/10.1039/d2gc03744k

‡ These authors contributed equally.

tions.[6] Recent observations suggest that the intact cellulose microfibrils should contain amorphous or disordered cellulose chains that are susceptible to acidic and enzymatic hydrolyses.[7,8] However, much remains unknown about the genesis and distribution of amorphous chains during cellulose synthesis and microfibril assembly in plant cell walls.

Cellulose synthase complexes (CSCs) are principally assembled on the plasma membranes of plant cells for the catalyzation of cellulose biosynthesis.[9,10] As a rosette-like structure with 6-fold symmetry, the CSCs putatively consist of 18–24 catalytic cellulose synthase (CESA) subunits.[11–13] In the two model plants, *Arabidopsis* and rice, several CESAs isoforms have been identified for cellulose biosynthesis of the primary cell walls; the other three isoforms (CESA4, CESA7, CESA8/A9) are required as essential components of CSCs for the synthesis of the secondary cell walls.[14,15] Although active CSCs have been developed *in vitro* for cellulose biosynthesis,[16,17] it is still unclear how functional CSCs produce distinct cellulose microfibrils.

Cellulose microfibrils are increasingly implemented to generate functional cellulose nanofibrils and nanocrystals as digestible substrates and convertible intermediates for diverse bioproduction.[18] Nevertheless, lignocellulose recalcitrance is responsible for the costly enzymatic hydrolysis of intact cellulose microfibrils, which has been assessed as a crucial limitation factor for producing high-yield sugars and high-value bioproducts.[19] As a promising solution, genetic engineering of cellulose biosynthesis has been conducted to improve lignocellulose recalcitrance in genetic mutants and transgenic crops. For instance, a natural rice mutant (*Osfc16*/*cesa9*) with site-mutation of OsCESA9 has been characterized with remarkably enhanced biomass enzymatic saccharification owing to its significantly reduced cellulose crystalline index (CrI) and degree of polymerization (DP). Importantly, the *Osfc16* mutant shows normal plant growth with significantly increased biomass yield and lodging resistance.[20] More recently, the *Osfc16* mutant has been applied to generate length-reduced cellulose nanofibrils as an inducing substrate at low dosage to facilitate *T. reesei* secretion of high-activity cellulases.[21]

Rice is an important food crop worldwide with large amounts of lignocellulose residues that are convertible for biofuels and biochemicals.[22] In this study, we performed a classic CRISPR/Cas9 gene editing to select distinct site-mutants and knockout lines of three OsCESA4,7,9 isoforms essential for the cellulose biosynthesis of secondary cell walls in rice. This study then determined the significantly altered cellulose features that are distinctive at the site-mutants and knockout lines, and observed the *in situ* length-reduced cellulose nanofibril assembly scaled by the high density of the amorphous cellulose chains. Employing those representative cellulose nanofibrils as substrates, we further detected either remarkably increased sugar yield released from enzymatic hydrolysis or improved lignocellulose-degradation enzymes secreted from incubation with the *T. reesei* strain, as well as size-reduced cellulose nanocrystals from acid modification. Taken together, the evidence thus suggests a novel strategy for producing high-yield sugars, high-quality nanocrystals, and high-activity cellulases by integrating genetic modification of cellulose nanofibrils with the green biomass process.

2. Materials and methods

2.1. Rice mutant selection

Diverse *oscesa* mutants and corresponding rice cultivar (*Oryza sativa*, *japonica* cultivar Nipponbare/NPB) as wild type (WT) were used to investigate the mechanism of OsCESAs complexes for cellulose nanofibrils assembly and bioproduction. All *oscesa* mutants, including site-mutations and knockouts, were generated by CRISPR-Cas9 gene-editing system.[23,24] The sgRNAs targeting *OsCESA4*,*7*,*9* were designed using the CRISPR-PLANT program,[25] and the corresponding oligonucleotides were used for plasmid construction (Table S1†). The oligonucleotides were cloned into the pRGEB32 or pCSGAPO1 vector, and transformed into rice WT calli *via Agrobacterium tumefaciens* strain EHA101. Specific primers (Table S1†) were used for the mutant screen by amplifying the genomic regions covering the target sites and sequential Sanger sequencing. Potential off-target sites of the homozygous lines were identified based on predictions by the CRISPR-P program.[26] Specific primers (Table S2†) were used for the plant off-target test by sequencing six to eight top-ranked potential off-target sites. All rice mutants were selected and grown in the experimental fields of Huazhong Agricultural University, Wuhan, China.

2.2. Biomass sample collection

Six biomass samples from various plant species were used as substrates for enzymatic hydrolysis by *T. reesei* strain secreted cellulases. Wheat, corn, eucalyptus, fern, reed, and rapeseed were among the plant species collected from experimental fields at Huazhong Agricultural University and Hunan Agricultural University. Plant mature stem tissues were dehydrated at 55 °C, cut into small pieces, ground through a 40-mesh screen (0.425 × 0.425 mm), and stored as biomass powders samples for cell wall polymer levels and feature analyses.

Rice stem tissues were cross-sectioned for *in situ* AFM analysis of cellulose nanofibrils. The bottom regions of the 2nd internodes were collected at the heading stage, and embedded in 4% agar. The cross-sections were then cut in half at 80 μm thick by a microtome (VT1000S, Leica). In a vacuum, the slices were immobilized on the mica surface. The immobilized slices were examined under a bright field light microscope, and the intact slices that exposed the innermost surface of the cell wall were chosen for further AFM analysis.

2.3. Extraction and determination of wall polymers

Unless otherwise specified, all chemicals and reagents were purchased from Sigma-Aldrich (St Louis, MO). The plant cell wall fractionation method was carried out as described earlier, with minor changes.[27,28] Using potassium phosphate buffer (pH 7.0), chloroform–methanol (1 : 1, v/v), DMSO–water (9 : 1,

v/v), and ammonium oxalate 0.5% (w/v), the lignocellulosic biomass was extracted sequentially to remove soluble sugars, lipid, starch, and pectin. The remaining residues were further extracted with 4 M KOH (added 1.0 mg mL^{-1} sodium borohydride) at 25 °C for 1 h, and the supernatants were defined as the KOH-extractable hemicellulose fraction. The remaining residue was used to detect the total pentoses for the non-KOH-extractable hemicellulose fraction. The total hemicellulose content was measured by counting the pentoses of the non-KOH-extractable residue, and the total hexoses and pentoses in the KOH-extractable supernatant. The *Updegraff* method was used to determine the contents of crystalline cellulose.[29] Colorimetric methods were used to determine hexoses and pentoses.[28] The total lignin content was measured using the two-stage sulfuric acid degradation method according to the National Renewable Energy Laboratory's Laboratory Analytical Procedure.[30] The GC-MS technique (Shimadzu GCMS-QP2010 Plus) was used to identify the ratio of arabinose to xylose in different hemicellulose extractions, as described previously.[28]

2.4. Detection of wall polymer features

The cellulose degree of polymerization (DP) was measured by the viscosity method, as described previously.[31] The *Updegraff* method was used to extract crystalline cellulose.[29] The experiment was conducted at 25 ± 0.5 °C with a water bath. Cupriethylenediamine hydroxide (Cuen) was used as the cellulose solvent in the Ubbelohde viscometer. The relative viscosity was represented by the ratio of t/t_0, where t and t_0 are the efflux times of the cellulose solution and Cuen (blank) solvent, respectively. The intrinsic viscosity was calculated refers to the United States Pharmacopeia table (USP, 2002) that files the predetermined values of the product of intrinsic viscosity and concentration. The cellulose DP was calculated by the equation: $DP^{0.905} = 0.75[\eta]$, where $[\eta]$ is the intrinsic viscosity of the solution calculated by interpolation using the USP table. All experiments were carried out in biological triplicate.

The lignocellulosic biomass crystallinity index (CrI) was determined by X-ray technique (XRD) (Rigaku-D/MAX, Ultima III; Japan), as described earlier.[28] The XRD scans 2θ from 5° to 45° to collect diffraction data for the calculation of CrI using the equation:

$$\mathrm{CrI}(\%) = \frac{I_{200} - I_{\mathrm{am}}}{I_{200}} \times 100$$

where I_{200} is the intensity of the 200 peaks at 2θ around 22.5° that represent the total intensity, while I_{am} is the amorphous cellulose intensity at 2θ around 18°.

2.5. Measurement of biomass porosity

Micrometrics ASAP 2460 (USA) was utilized to investigate the cellulosic matrix pore size distribution, as previously stated.[32] The intact cellulose microfibrils were obtained by the 8% $NaClO_2$ treatment described in **2.6**. Using the Horvath–Kawazoe (HK) and the Barrett–Joyner–Halenda (BJH) approaches, the distribution of micropore and nanopore volumes was determined.

2.6. Preparation of cellulose microfibrils and nanofibrils

Acidic chlorite treatments were used for the removal of lignin, as described in our previously established method with modification.[33] First, 1 mN HCl was added to 1 g sodium chlorite ($NaClO_2$) to provide an acidic environment. The stem tissue section slices were incubated with different concentrations of acidic sodium chlorite (8% as mild treatment and 16% as harsh treatment, w/v) at 50 °C for 2 cycles (24 h per cycle). Excessive chlorite was used for slice samples. After each cycle of treatment, the samples were washed with ultrahigh purity water until neutral pH was achieved. The slice samples were dried in a vacuum environment for further AFM studies.

2.7. Atomic force microscopy (AFM) observation

AFM imaging was applied for the observation of the cellulose microfibrils and nanofibrils ultrastructure.[33] The AFM tips were acquired from Nanoscience Instruments (Phoenix, Arizona), and have a nominal spring constant of roughly 0.1 N m^{-1} (CS-25 silicon, Lot: AP50152). The Agilent multifunctional AFM scanner with open-loop was used for all imaging, and the PicoPlus Molecular Imaging system with a PicoScan 3000 Controller was used. To reduce outside noise, the entire system was mounted on the PicoPlus Isolation Chamber. The non-contact, top magnetic AC (TopMAC) mode was used to capture the topography (height) photographs. All samples were photographed with 512 × 512 pixels and an average scanning speed of 1 ln per s. To ensure repeatability, at least three independent tests were also carried out. A total of 100 data points and around 10 randomly selected zoom-in areas were gathered for statistical analysis. Gwyddion software (2.56 version) was used for AFM data visualization and analysis.

2.8. Biomass enzymatic saccharification assay

The biomass enzymatic saccharification was performed after lime (CaO) pretreatment, as previously described.[34] The biomass powders (0.3 g) were added into 6 mL 5% CaO (w/w). The sealed samples were incubated at 50 °C, shaken at 150 rpm for 48 h, and centrifuged at 3000*g* for 5 min. The pellets were washed with 10 mL distilled water until reaching a pH value of 7.0, and once with 0.2 M phosphate buffer at pH 4.8. The samples were then incubated with 1.6 g L^{-1} mixed-cellulases (HSB) with final concentrations of cellulases at 10.60 FPU per g biomass and xylanase at 6.72 U g^{-1} biomass with 5% solid loading. During enzymatic hydrolysis, the samples were co-supplied with 1% Tween-80 and shaken under 150 rpm at 50 °C for 48 h. After the reaction, the samples were centrifuged at 3000*g* for 5 min, and the precipitation was collected to assay the remaining un-digested cellulose. The percentage of digested cellulose was calculated to account for the hexose yield released from enzymatic hydrolysis. All experiments were carried out in independent triplicate.

2.9. Preparation of cellulose nanocrystals

A concentrated sulfuric acid hydrolysis method was applied to produce the cellulose nanocrystals, as previously

described.[35,36] Firstly, crude cellulose was prepared. The biomass sample was de-lignified with 8% $NaClO_2$ as described above with a solid ratio of 1 : 50 (w/v), and hemicelluloses were further removed with 5% NaOH (w/v) at 50 °C for 1 h (5 times). After that, the samples were washed five times with deionized water, twice with pure methanol, twice with anhydrous acetone, dehydrated in the hood overnight, and dried in a 50 °C oven for 2 hours. Secondly, crude cellulose was hydrolyzed and the cellulose nanocrystal colloidal solution was obtained. The crude cellulose was hydrolyzed by 64% sulfuric acid (w/w) with a solid ratio of 1 : 20 (w/v) at 45 °C for 1.5 hours in a 40 kHz ultra-wave. After stopping the acid hydrolysis with 10-fold chilled distilled water, the sample was centrifuged at 6000*g* for 5 minutes to remove excess acid. The remaining pellets underwent dialysis for three days with membranes with a molecular weight cutoff of 14 000 Da. To avoid nanocrystal particle aggregation, the colloidal solution was sonicated for 15 minutes before sample preparation. For AFM observation, the final nanocrystal colloidal was diluted to 0.001% (w/w) with ultrahigh purity water and thoroughly shaken.

2.10. Cellulases assay secreted by fungi

The cellulose nanofibrils extracted from the biomass samples were applied as inducing substrates to incubate with the *T. reesei* (Rut-C30, CICC40348) strain for cellulase secretion. A combination of hot alkaline extraction followed by a high-pressure homogenization with 20 cycle times (HPH, AH-1500, ATS, Canada) was conducted to extract the nanofibrils substrates,[37] and *T. reesei* was incubated with 0.12 g cellulose nanofibrils in 30 mL liquid culture, as described previously.[38] After incubation for 7 days, the culture media were centrifuged at 3000*g* for 10 min to collect supernatants as secreted crude cellulase enzymes. Cellulase activity and protein level assays were carried out, as previously described.[38] The proteome of the crude secreted cellulases was analyzed by LC-MS/MS (Orbitrap Elite LCMS/MS, Thermo, USA), and the data were identified by searching the protein sequence databases downloaded from Uniprot (**https://www.uniprot.org**), as previously described.[38]

For biomass enzymatic saccharification using the secreted crude cellulases, the biomass samples were pretreated with 5 mL 0.5% NaOH (w/v) under 150 rpm shaken at 50 °C for 2 h. The pretreated biomass residues were incubated with 10 FPU per g of the secreted crude cellulases by *T. reesei*. Enzymatic hydrolysis reactions were conducted as described above. All experiments were performed in independent triplicate.

2.11. Statistical analysis

Spearman correlation analyses of major wall parameters were performed by IBM SPSS Statistics 26 software with two-tailed significance ($^*P < 0.05$, $^{**}P < 0.01$). Significant differences between the WT and mutant were determined with a two-tailed Student's *t*-test ($^{**}P < 0.01$, $^*P < 0.05$) by Microsoft Excel 2016. Quantitative data are expressed as average ± standard deviation (SD), and the replication was noted in each experiment.

3. Results and discussion

3.1. Distinctively altered cellulose features in site-mutants and knockout lines

As OsCESA4, OsCESA7 and OsCESA9 are the essential isoforms of CSCs for cellulose biosynthesis of the secondary cell walls in rice,[14] this study selected four site-mutants and three knockout lines of three OsCESA4,7,9 isoforms by conducting a classic CRISPR/Cas9 gene editing with a japonica rice cultivar (Nipponbare/NPB), which were verified by whole-genome sequencing and genetic segregation analyses (Fig. S1 and Table S1†). Although site mutations occurred in various functional domains of OsCESAs, including the N-/C-terminal and middle regions, all present site-mutants exhibited slightly defective plant growth phenotypes (Fig. S1a†). As a comparison with wild type/WT (NPB), the site-mutants were measured with varied grain and biomass yields, but the three knockout lines exhibited severe growth-defective and seed semi-lethal phenotypes (Fig. S1a†), which should confirm the previous assumption that all three CESAs isoforms are essential for cellulose biosynthesis in rice. Hence, the site mutations of the three CESA isoforms should be a powerful approach for the selection of desirable bioenergy crops, whereas their knockout lines could be applicable to generate specified lignocellulose substrates. Using our previously established approaches,[28] this study determined the major wall polymer composition and features of all seven site-mutants and knockout lines in their mature straws (Fig. 1). Compared with the WT, all site-mutants contained significantly lower cellulose levels by 22%–35% at $P < 0.01$ levels ($n = 3$), whereas the three knockout lines showed cellulose contents reduced by 51%–59% (Fig. 1a). Conversely, the hemicellulose and lignin contents were not altered much in the site-mutants and knockout lines (Fig. 1b and c), suggesting that genetic engineering of *OsCESAs* genes should mainly affect cellulose biosynthesis. In terms of the two major cellulose features, this work further detected much-reduced cellulose CrI and DP values in the site-mutant and knockout lines (Fig. 1d and e), consistent with the findings examined in the *Osfc16* mutant.[20] Xylan is a major hemicellulose, and the substituted arabinose (Ara) of non-KOH-extractable xylan has been assumed to tightly associate with cellulose microfibrils in rice.[3] Thus, this study examined the significantly increased Ara/Xyl ratios in the site-mutants and knockout lines relative to WT (Fig. 1f). The results suggested that the cellulose microfibrils of all site-mutants should be from more amorphous regions that more readily interacted with the xylan sidechains. It is thus assumed that cellulose nanofibers could be also accountable by the branched hemicellulose interactions in the site-mutants examined. In addition, all site-mutants and knockout lines showed slightly altered Ara/Xyl values in the KOH-extractable hemicelluloses, which should consist of more than 70% of the total hemicelluloses in rice (Fig. S2†). Taken together, genetic manipulation of the three OsCESAs isoforms could predominately modify the cellulose levels and features, and also affect the minor non-KOH-extractable xylan in plant cell walls of mature rice straws.

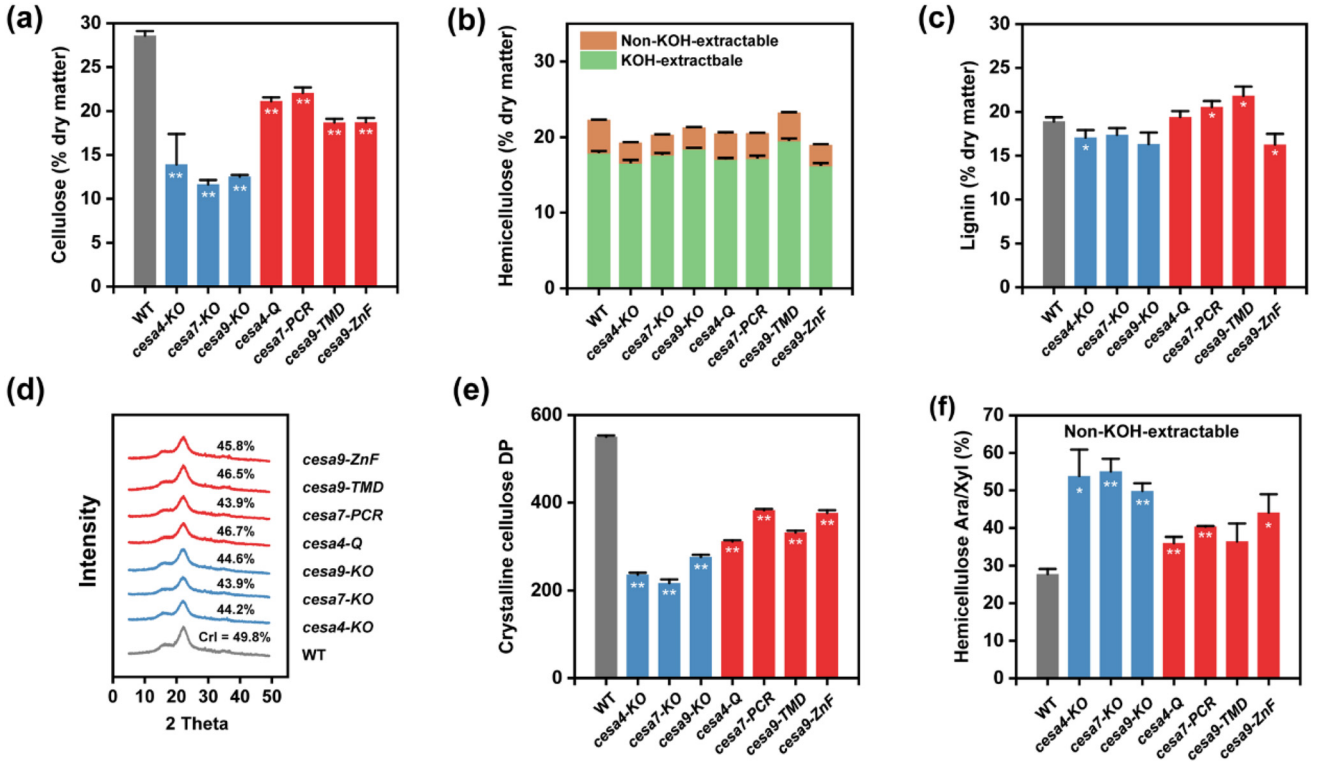

Fig. 1 Cell wall polymer levels and features of site-mutants and knockout lines of OsCESA4,7,9 isoforms. (a) Cellulose content. (b) Hemicellulose content. (c) Lignin content. (d) Lignocellulosic CrI of mature stem. (e) Crystalline cellulose DP. (f) The ratio of arabinose to xylose in non-KOH-extractable hemicelluloses. Data as means ± SD (n = 3) in (a, b, c, e and f); significant differences between the WT and mutant were determined using two-tailed Student's t-test: $^{**}P < 0.01$, $^{*}P < 0.05$.

3.2. Distinct length-reduced cellulose nanofibrils assembly

To understand the specific alteration of the cellulose levels and features in the site-mutants and knockout lines, this study attempted to explore the *in situ* cellulose nanofibrils assembly by exposing the native cellulose microfibrils from lignin and hemicellulose coextraction with different concentrations of $NaClO_2$ (Fig. 2). By means of our recently established AFM technique,[33] we observed a typically crossed cellulose microfibril orientation with a distinctive direction on each cell wall lamella in the WT after 8% $NaClO_2$ extraction, consistent with the previous reports in other tissues (Fig. 2a).[39,40] As a com-

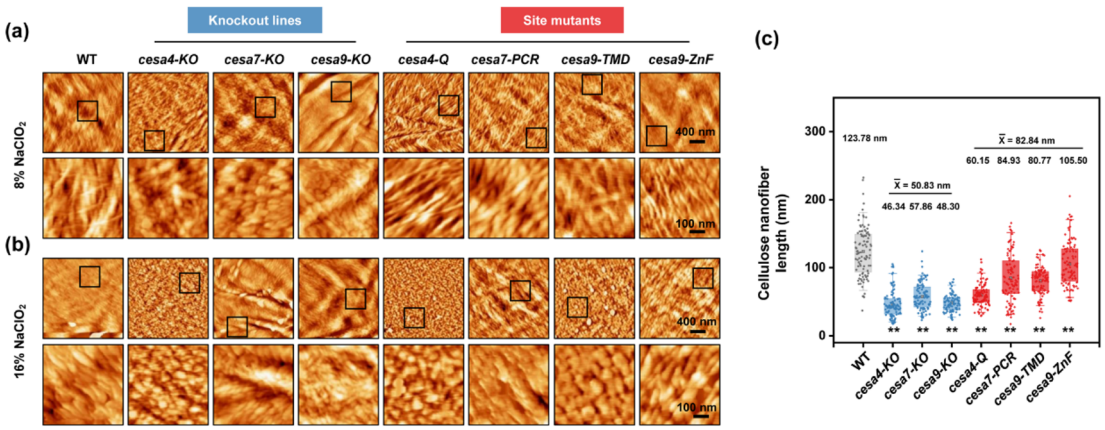

Fig. 2 Distinct cellulose nanofibril assembly *in situ* in rice site-mutants and knockout lines compared to wild type. (a and b) AFM observations *in situ* of stem tissues after 8% and 16% $NaClO_2$ extractions. The areas in the black boxes are magnified in the lower images. (c) Estimation of average cellulose nanofiber lengths from random selections of 100 nanofibrils. Data in (c) are displayed as box and whisker plots with individual data points. The error bars represent 95th and 5th percentiles. Centerline, average; box limits, 25th and 75th percentiles. Significant differences between the WT and mutant were determined using two-tailed Student's t-test: $^{**}P < 0.01$, $^{*}P < 0.05$.

parison, all site-mutants started to exhibit cellulose microfibril assembly with the tangled formation at a small angle, but three knockout lines clearly showed cellulose nanofibril accumulation (Fig. 2a). This is consistent with their observed reduction in cellulose DP values (Fig. 1e). By further performing 16% $NaClO_2$ extraction, we could observe the cellulose nanofibril assembly in all of the examined samples, and estimated the lengths of cellulose nanofibrils by scaling the average distances between two amorphous/defective/non-crystalline cellulose chains among the 100 randomly-selected cellulose nanofibrils (Fig. 2b). Compared to the WT with an average cellulose nanofibril length at 123.78 nm, the site-mutants and knockout lines showed the average nanofibril lengths at 82.84 nm and 50.83 nm, respectively (Fig. 2c). Despite the various cellulose nanofibrils lengths examined, the three knockout lines retained significantly shorter nanofibrils than the site-mutants, consistent with their examined distinct cellulose DP values (Fig. 1e). The results thus implicate that the genetic engineering of the OsCESA4,7,9 isoforms could cause length-reduced cellulose nanofibril assembly, accounting for the high density of the amorphous cellulose chains accumulation in the plant cell walls.

3.3. Remarkably increased biomass saccharification under mild chemical pretreatment

As amorphous cellulose is susceptible to enzymatic and chemical digestion,[41] this study examined whether the high density of amorphous cellulose chains could enhance the biomass enzymatic saccharification in the site-mutants and knockout lines. Using our previously established method, we measured the hexose yields (% cellulose) released from enzymatic hydrolyses after alkali pretreatments with four representative biomass samples (Fig. 3). Without any pretreatment, all four representative samples showed significantly higher hexose yields than those of the WT by 46%–70% from the direct enzymatic hydrolyses of mature rice straws. Under 5% CaO pretreatment, a mild and chemically recyclable process, the four samples showed almost complete cellulose digestions with hexose yields close to 100%. In contrast, the WT had the hexose yield at less than 70%, suggesting that the length-reduced cellulose nanofibrils should be the desirable substrates for high biomass enzymatic saccharification. Hence, provided that the reduced cellulose features (CrI, DP) indicate the much-improved lignocellulose recalcitrance for high biomass enzymatic saccharification in the natural *Osfc16* mutant,[20] this study further indicated that the amorphous cellulose chains should directly account for the biomass digestibility in bioenergy crops.

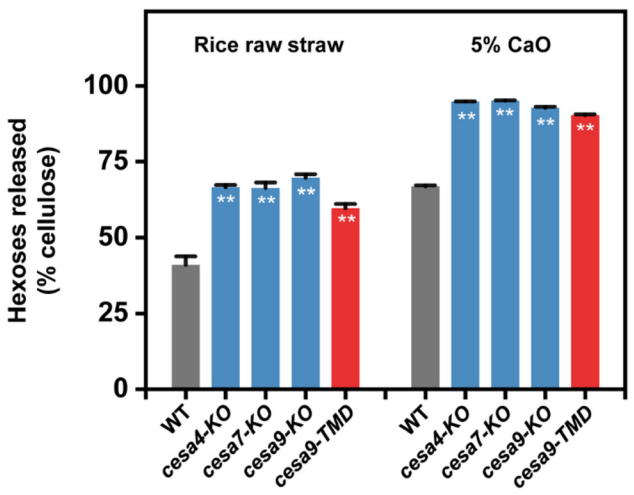

Fig. 3 High enzymatic saccharification *in vitro* in rice site-mutants and knockout lines compared to wild type. Hexose yields were released from enzymatic hydrolyses of mature rice straws after 5% CaO pretreatment. Data as means ± SD (n = 3). Significant differences between the WT and mutant were determined using two-tailed Student's t-test: $^{**}P < 0.01$, $^{*}P < 0.05$.

3.4. Characteristic size-reduced cellulose nanocrystals by typical acid catalysis

Since cellulose microfibrils have been applied to generate cellulose nanofibrils as the functional intermediates for highly-valuable bioproduction,[18] this study obtained fully-separated cellulose nanocrystals *in vitro* by treating cellulose microfibrils with 64% H_2SO_4 (w/w, 45 °C) in site-mutants and knockout lines (Fig. 4). Because sulfuric acid treatment is well known for efficiently cleaving off all surface and inner amorphous cellulose chains from the entire cellulose microfibrils,[18] we observed distinct spindle-like cellulose nanocrystals generated in all samples under AFM (Fig. 4a). We then estimated the average sizes of 100 randomly-selected cellulose nanocrystals (Fig. 4b and c). As a result, the WT produced cellulose nanocrystals at 219.43 nm length and 7.98 nm diameter, whereas the site-mutants and knockout lines could generate significantly smaller sizes of nanocrystals with average lengths reduced by 23%–43% and diameters reduced by 21%–28%. Meanwhile, all knockout lines retained smaller nanocrystal sizes than the site-mutants at $P < 0.05$ (n = 100) *in vitro*. This is consistent with their length-reduced cellulose nanofibrils assembly observed *in situ*. Notably, the same diameter of nanocrystals was measured in the three knockout lines, providing evidence for an equal proportion of the three OsCESA4,7,9 isoforms for CSC construction. Hence, the three OsCESA4,7,9 isoforms should be equally functional for cellulose production in rice.

As the size-reduced cellulose nanocrystals are defined as high-quality intermediates for bioproduction,[42] this study estimated the reducing rates of the cellulose nanocrystals generated from the cellulose microfibrils of the site-mutants and knockout lines (Fig. 4d). The cellulose microfibrils of the site-mutants and knockout lines were most effective in generating small-sized nanocrystals without additional processes. In contrast, the common cellulose substrates have been observed to require more energy-consuming treatments for relatively low-efficiency nanocrystal production in previous studies (Fig. 4d and Table 1).[35,43–47] As the lengths of the nanocrystals generated from the H_2SO_4 treatment *in vitro* remained much longer than those of the cellulose nanofibrils measured *in situ* in all

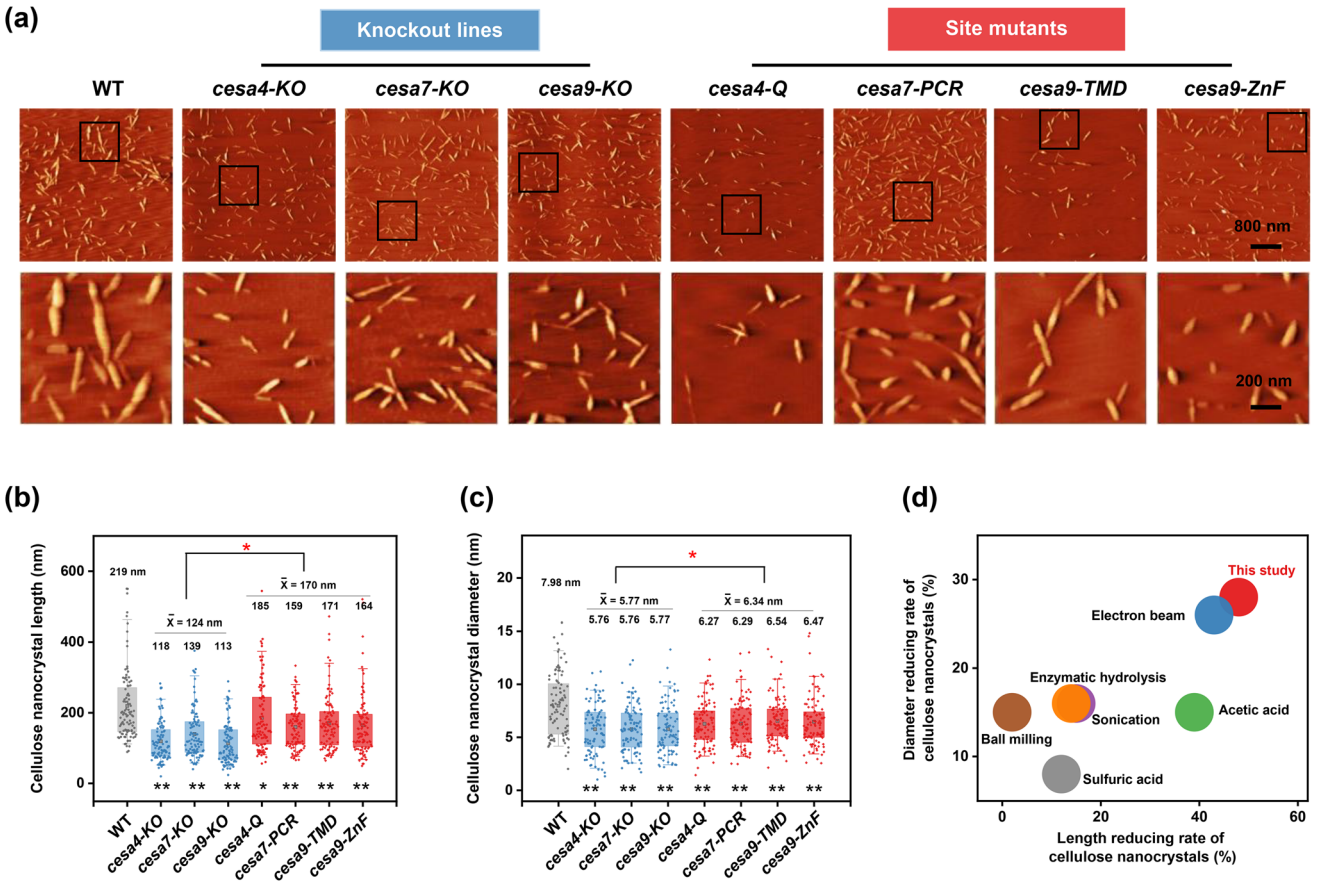

Fig. 4 Assorted cellulose nanocrystals generated from knockout lines and site-mutants of OsCESA4,7,9 complexes. (a) AFM observation of cellulose nanocrystals. The areas in the black boxes are magnified in the lower images. (b and c) Measurement of the average length and diameter of the nanocrystals by random selection of 100 nanocrystals. (d) Comparison of the dimension (length, diameter) reducing rates of nanocrystals generated from genetically-modified cellulose microfibrils in this study and common microfibrils examined in previous studies. Data in (b) and (c) are displayed as box and whisker plots with individual data points. The error bars represent the 95th and 5th percentiles. Centerline, average; box limits, 25th and 75th percentiles. Significant differences between the WT and mutant were determined using two-tailed Student's *t*-test: $^{**}P < 0.01$, $^{*}P < 0.05$. Detailed information of (d) is listed in Table 1.

Table 1 Comparison of cellulose nanocrystals generated from modified microfibrils in this study and common microfibrils examined in previous studies

Source	Method	Length (nm)	Diameter (nm)	Length reducing rate (%)	Diameter reducing rate (%)	Additional process	Ref.
Genetically engineered rice straw	**Classic sulfuric acid hydrolysis**	**113**	**5.76**	**48%**	**28%**	**Not required**	**This study**
Black spruce	Concentrated sulfuric acid hydrolysis	105	4.5	12%	8%	8.75 mL 64% sulfuric acid per 1 g cellulose	35
Softwood	Enhanced electron beam irradiation	128	23	43%	26%	500 kGy radiation dosage per 10 g cellulose	43
Eucalyptus	Additional acetic acid hydrolysis	175	12	39%	15%	10 mL acetic acid per 3 g cellulose	44
MCC	Prolonged sonication	163	4.6	15%	16%	90 min Prolonged ultrasonication (19.5 kHz, oscillation amplitude of 90%)	45
Sugarcane bagasse	Prolonged enzymatic hydrolysis	352	8.4	14%	16%	1 day Prolonged for enzymatic system	46
Avicel PH-101	Prolonged ball milling	424	17	2%	15%	45 min Prolonged for ball milling (1000 rpm)	47

samples examined, it justified the previous assumption that the intact cellulose microfibrils should contain the long crystalline cellulose cores that are undigested by this H_2SO_4 treatment. It also suggests that the cellulose microfibrils of the site-mutants and knockout lines are of inner-broken cellulose chains removable by the H_2SO_4 treatments for diameter-reduced nanocrystals distinctive in WT, site-mutants, and knockout lines.

3.5. Length-reduced cellulose nanofibrils as effective substrates for high-activity cellulases production

Because the cellulose nanofibrils of the natural *Osfc16* mutant at low dosage have been co-supplied with lignocellulose substrates for enhancing the *T. reesei* strain secretion of cellulases,[21] this study further applied the homogenized nanofibrils of one representative site-mutant (*cesa9-TMD*) as the only carbon source to incubate with the *T. reesei* strain for the production of lignocellulose-degradation enzymes (Fig. 5). In general, the protein level and cellulase activity secreted by the *T. reesei* strain were significantly higher in the site-mutant sample at the $P < 0.01$ level than the WT, with increased protein level by 44% and cellulase activity by 26% (Fig. 5a and b). Furthermore, different types of enzymes were identified, including exoglucanases (CBHs), endoglucanases (EGs), β-glucosidases (BGs), and xylanases (Table S3†). In particular, the CBHI (pNPC) and BG activities induced by the site-mutant sample were increased by 100% and 138% compared with the WT sample (Fig. 5c and d), respectively. Upon further supplying secreted crude enzymes into the biomass hydrolyses of seven major bioenergy crops *in vitro*, the site-mutant sample retained consistently higher hexose yields than the WT sample at $P < 0.01$ levels (Fig. 5e). The results thus suggest that the length-reduced cellulose nanofibrils of the site-mutant should bear more breakpoints for initiating and accelerating fungi attack to digest cellulose into glucose as its carbon source, and then enabling the increase of the cellulase secretion. This is consistent with our previous report that the cellulose nanofibrils generated from the natural *Osfc16* mutant could act as an effective inducer for enhancing the *T. reesei* secretion of cellulase complexes.[21] However, even though this study selected the representative site-mutant (*cesa9-TMD*) for high cellulase production, the site-mutant and/or knockout line must still be optimized to obtain the maximum lignocellulose-degradation enzyme secretion by *T. reesei* incubation with distinct cellulose nanofibrils substrate in the future.

3.6. Engineered cellulose microfibrils are rich with micropores and nanopores

To understand why the site-mutants and knockout lines showed much improved lignocellulose recalcitrance for high-quality nanocrystals and high-yield bioproduction (sugars and cellulases) as examined above, we measured the pore size and distribution of cellulosic microfibrils by the N_2 adsorption/desorption method (Fig. 6). Compared with the WT, all site-mutants and knockout lines contain remarkably increased numbers of micropores (2–50 nm) and nanopores (<2 nm) by up to 2–4 folds in the microfibrils, but the knockout lines retained greater micro- and nanopore distributions than the site-mutants. Further analysis indicates a significantly negative correlation between the nanopore (1 nm) volumes and cellulose nanocrystal lengths or nanofibril lengths (Table S4†), indicatingg that the increased nanopores should be primarily derived from the inner-broken cellulose chains and surface amorphous cellulose chains in the site-mutants and knockout lines. This result also suggests that the micropore distribution mainly occur among the wall polymer interaction networks.

3.7. Mechanism of distinct cellulose nanofibril assembly for improved biomass saccharification and bioproduction

By exposing the native cellulose microfibrils from mild lignin and hemicellulose co-extraction, this study has applied classic AFM to sort out the distinct cellulose nanofibril assembly *in situ* and cellulose nanocrystal production *in vitro* in the site-mutants and knockout lines of the three OsCESA4,7,9 isoforms. This led to a hypothetic model about the three major types of functional CSCs that are favored for the characteristic

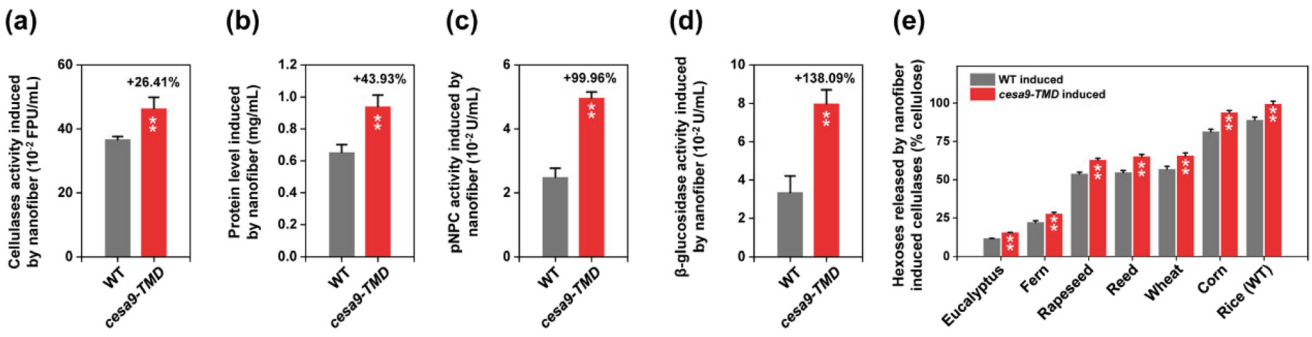

Fig. 5 Notably enhanced cellulase production secreted by *T. reesei* strain after incubation with the homogenized nanofibrils of WT and one site-mutant (*cesa9-TMD*). (a) General cellulase activity *in vitro*. (b) Total protein level. (c) pNPC activity for CBH activity. (d) BG activity. (e) Hexose yields (% cellulose) released by enzymatic hydrolyses of mature straws in five bioenergy crops after 0.5% NaOH pretreatments by supplying crude enzymes secreted by the *T. reesei* strain. Data in (d) as means ± SD ($n = 3$). Significant differences between the WT and mutant were determined using two-tailed Student's *t*-test: $^{**}P < 0.01$, $^{*}P < 0.05$.

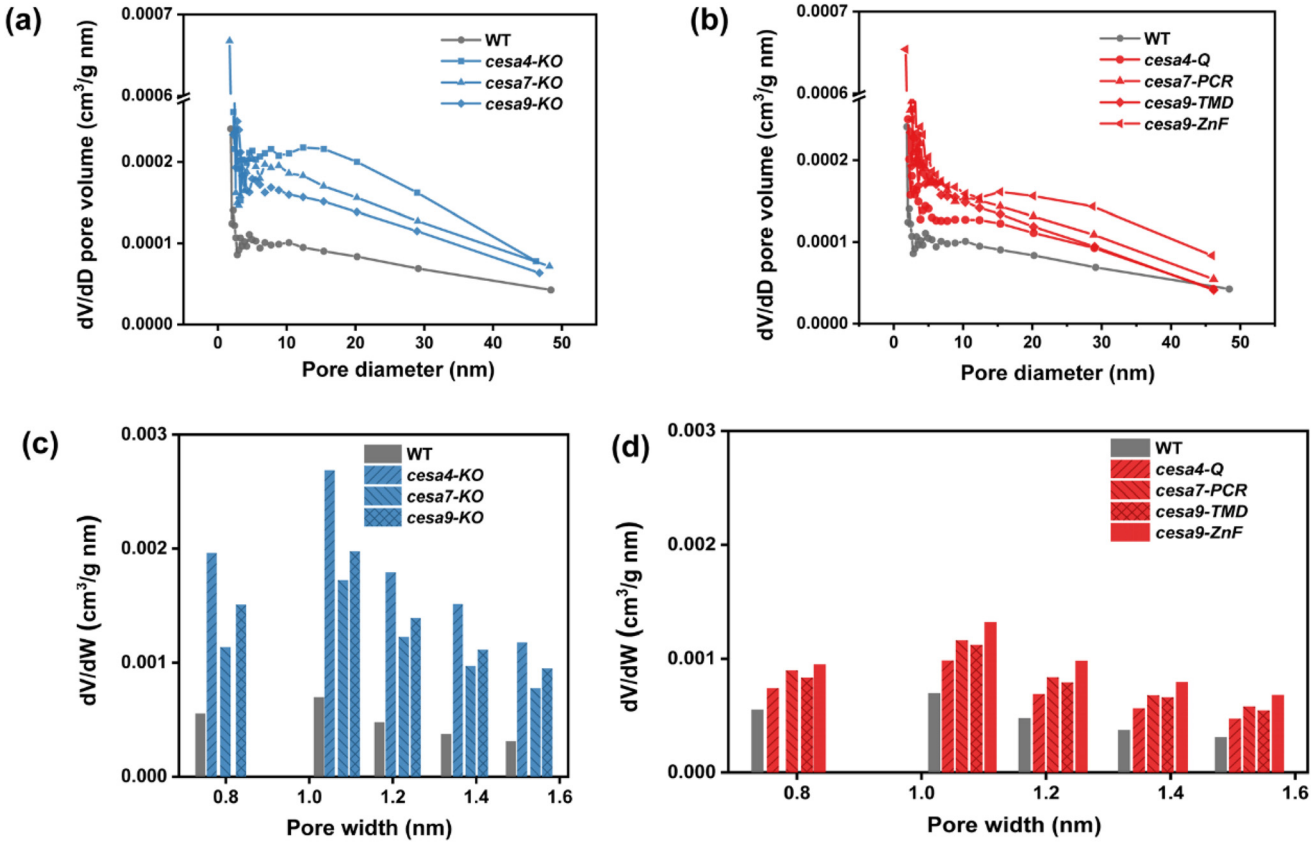

Fig. 6 Systemically raised nanopore volumes of intact cellulose microfibrils in knockout lines and site-mutants after 16% $NaClO_2$ extraction. (a and b) BJH adsorption micropore distribution. (c and d) Horvath-Kawazoe nanopore distribution.

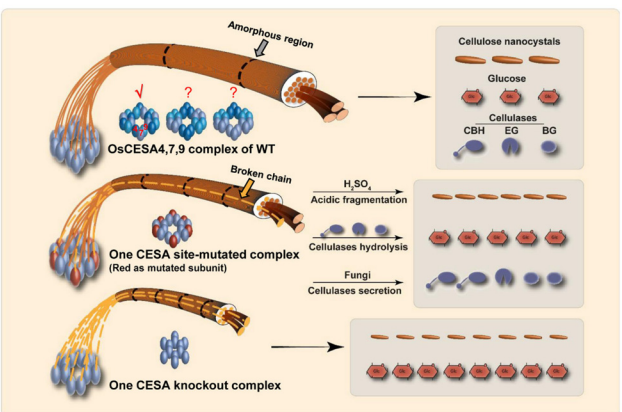

Fig. 7 A novel model for the genetic engineering of OsCESA4,7,9 complexes for distinct cellulose nanofibril assembly accountable for amorphous/non-crystalline/disorganized cellulose chain distributions. These are defined as breakpoints or native weakness of the microfibrils for initiating and facilitating enzymatic hydrolysis into glucose, acidic fragmentation into cellulose nanocrystals, and fungi attack to secret cellulase production.

cellulose microfibril accumulation into plant cell walls (Fig. 7). Even though PttCESA8/GhCESA7 has been recently constructed as an active homotrimeric complex *in vitro*,[16,17] this model indicates that each isoform of OsCESA4,7,9 is not replaceable for CSC construction in plant cells. Hence, each isoform should be independently functional for cellulose nanofibril assembly in plant cell walls *in situ*. In particular, as the three knockout lines could produce cellulose nanocrystals of the same diameter (Fig. 4), the three OsCESA4,7,9 isoforms should form CSCs under equal proportion (1 : 1 : 1) and symmetric distribution. This may explain the previous observation that the overproduction of secondary wall CESAs causes a defective cell wall integrity.[48] As not all site-mutants showed abnormal amorphous cellulose assembly on the large surfaces of the microfibrils (Fig. 2), the three OsCESA4,7,9 isoforms are mostly likely to form heterotrimeric structures with symmetric CESA distribution in plant cells, which enables them to maintain the CSCs integrity in the site-mutants for slightly altered plant growth and biomass yields. By comparison, the integrity of the heterodimeric structure in the three knockout lines should not be stable, leading to the semi seed-lethal phenotype observed in this study. Although the site mutation of the CESAs complexes is applicable to improving the cellulose recalcitrance for remarkably enhanced biomass saccharification and bioproduction in bioenergy crops, the knockout of the CESA isoforms should provide extremely high-quality lignocellulose substrates for specific biomass utilization.

As CSCs are putatively assembled as a rosette-like structure that is perfect for β-1,4-glucan chains to form crystalline microfibrils in plant cell walls, it is commonly accepted that the amorphous cellulose chains should be derived from the post-modification of cellulose microfibrils, including microfibrils twisting and bending,[39,49,50] as well as hemicelluloses interaction.[51,52] However, this study has *in situ* observed length-reduced cellulose nanofibril assembly, accounting for the high density of amorphous cellulose chains in the site-mutants and knockout lines (Fig. 2). This provides solid evidence that cellulose biosynthesis is a crucial factor for amorphous cellulose formation in plant cell walls during plant growth and development.

Provided that the amorphous cellulose chains are accessible and digestible,[41] the mechanism model highlights the amorphous cellulose chains as breakpoints of intact cellulose microfibrils for initiating and completing enzymatic (cellulases) hydrolysis into glucose, chemical (acid) fragmentation into nanocrystals, and fungi invading to secret cellulases (Fig. 7). This model also indicates that the inner-broken cellulose chains should occur in the site-mutants and knockout lines due to their distinctively reduced diameters of cellulose nanocrystals from the acid modifications, and the different pore sizes and distributions of cellulosic microfibrils, which could consequently ensure the near-complete hydrolysis and conversion for greatly improved glucose yield, nanocrystal quality, and cellulase activity. Therefore, the model can interpret how the desirable cellulose nanofibrils are digestible and convertible.

4. Conclusions

By selecting site-mutants and knockout lines of three essential OsCESA4,7,9 isoforms for cellulose biosynthesis, this study has observed length-reduced cellulose nanofibril assembly, which should account for the high density of the amorphous cellulose chain accumulation in plant cell walls. As the amorphous cellulose chains act as the breakpoints for initiating and completing the enzymatic and chemical catalysis of cellulose digestion and conversion, this study has thus examined either the near-complete biomass enzymatic saccharification or size-reduced cellulose nanocrystals as the optimal intermediates for high-quality bioproduction. Meanwhile, the desirable cellulose nanofibrils could be directly applied to induce the *T. reesei* strain as a carbon source for secreting high-yield and high-activity lignocellulose-degradation enzymes. It thus provides an applicable strategy for the great improvement of biomass saccharification, cellulose nanocrystal quality, and cellulase activity by integrating precisely engineered cellulose nanofibrils with effective processing technology.

Author contributions

R. Z.: methodology, investigation, visualization, software, writing-original draft; Z. H.: methodology, investigation, software; H. P., P. L., Y. W., J. L.: software, investigation; Y. W., T. X., J. L.: supervision, project administration, funding acquisition; L. P.: conceptualization, supervision, methodology, writing–review and editing, project administration, funding acquisition.

Conflicts of interest

The authors declare no competing interests.

Acknowledgements

We thank Dr Jiankang Zhu and Dr Kabin Xie for kindly providing the CRISPR-Cas9 vectors, Professor Yun Wang for technical assistance, and Ms. Yuanyuan Chen for vector construction. This work was supported by the National Natural Science Foundation of China (32170268, 32100214), Project of Huazhong Agricultural University Independent Scientific & Technological Innovation Foundation (2662019PY054; 2662020ZKPY013), National 111 Project of Ministry of Education of China (BP0820035, D17009), and the Project of Hubei University of Arts & Science (XKQ2018006).

References

1 L. Brinchi, F. Cotana, E. Fortunati and J. M. Kenny, *Carbohydr. Polym.*, 2013, **94**, 154–169.
2 A. Dufresne, *Philos. Trans. R. Soc., A*, 2018, **376**, 20170040.
3 Y. T. Wang, C. F. Fan, H. Z. Hu, Y. Li, D. Sun, Y. M. Wang and L. C. Peng, *Biotechnol. Adv.*, 2016, **34**, 997–1017.
4 H. E. McFarlane, A. Doring and S. Persson, *Annu. Rev. Plant Biol.*, 2014, **65**, 69–94.
5 Y. Nishiyama, *J. Wood Sci.*, 2009, **55**, 241–249.
6 M. C. McCann and N. C. Carpita, *J. Exp. Bot.*, 2015, **66**, 4109–4118.
7 Y. Nishiyama, U. J. Kim, D. Y. Kim, K. S. Katsumata, R. P. May and P. Langan, *Biomacromolecules*, 2003, **4**, 1013–1017.
8 M. C. Jarvis, *Philos. Trans. R. Soc., A*, 2018, **376**, 20170045.
9 A. R. Paredez, C. R. Somerville and D. W. Ehrhardt, *Science*, 2006, **312**, 1491–1495.
10 L. C. Peng, Y. Kawagoe, P. Hogan and D. Delmer, *Science*, 2002, **295**, 147–150.
11 M. Kumar, L. Campbell and S. Turner, *J. Exp. Bot.*, 2016, **67**, 515–531.
12 J. K. Polko and J. J. Kieber, *Plant Cell*, 2019, **31**, 282–296.
13 R. Zhong, D. Cui and Z.-H. Ye, *New Phytol.*, 2019, **221**, 1703–1723.
14 K. Tanaka, K. Murata, M. Yamazaki, K. Onosato, A. Miyao and H. Hirochika, *Plant Physiol.*, 2003, **133**, 73–83.
15 N. G. Taylor, R. M. Howells, A. K. Huttly, K. Vickers and S. R. Turner, *Proc. Natl. Acad. Sci. U. S. A.*, 2003, **100**, 1450–1455.

16 P. Purushotham, R. Ho and J. Zimmer, *Science*, 2020, **369**, 1089–1094.
17 X. Zhang, Y. Xue, Z. Guan, C. Zhou, Y. Nie, S. Men, Q. Wang, C. Shen, D. Zhang, S. Jin, L. Tu, P. Yin and X. Zhang, *Plant Biotechnol. J.*, 2021, **19**, 1579–1587.
18 E. Kontturi, P. Laaksonen, M. B. Linder, Nonappa, A. H. Groschel, O. J. Rojas and O. Ikkala, *Adv. Mater.*, 2018, **30**, e1703779.
19 Y. M. Wang, P. Liu, G. F. Zhang, Q. M. Yang, J. Lu, T. Xia, L. C. Peng and Y. T. Wang, *Renewable Sustainable Energy Rev.*, 2021, **137**, 110586.
20 F. Li, G. Xie, J. Huang, R. Zhang, Y. Li, M. Zhang, Y. Wang, A. Li, X. Li, T. Xia, C. Qu, F. Hu, A. J. Ragauskas and L. Peng, *Plant Biotechnol. J.*, 2017, **15**, 1093–1104.
21 H. Peng, W. Y. Zhao, J. Y. Liu, P. Liu, H. Z. Yu, J. Deng, Q. M. Yang, R. Zhang, Z. Hu, S. L. Liu, D. Sun, L. C. Peng and Y. T. Wang, *Green Chem.*, 2022, **24**, 2975–2987.
22 L. Dominguez-Escriba and M. Porcar, *Biofuels, Bioprod. Biorefin.*, 2010, **4**, 154–159.
23 Y. M. Lu and J. K. Zhu, *Mol. Plant*, 2017, **10**, 523–525.
24 K. B. Xie, B. Minkenberg and Y. N. Yang, *Proc. Natl. Acad. Sci. U. S. A.*, 2015, **112**, 3570–3575.
25 K. B. Xie, J. W. Zhang and Y. N. Yang, *Mol. Plant*, 2014, **7**, 923–926.
26 H. Liu, Y. D. Ding, Y. Q. Zhou, W. Q. Jin, K. B. Xie and L. L. Chen, *Mol. Plant*, 2017, **10**, 530–532.
27 L. C. Peng, C. H. Hocart, J. W. Redmond and R. E. Williamson, *Planta*, 2000, **211**, 406–414.
28 N. Xu, W. Zhang, S. F. Ren, F. Liu, C. Q. Zhao, H. F. Liao, Z. D. Xu, J. F. Huang, Q. Li, Y. Y. Tu, B. Yu, Y. T. Wang, J. X. Jiang, J. P. Qin and L. C. Peng, *Biotechnol. Biofuels*, 2012, **5**, 58.
29 D. M. Updegraff, *Anal. Biochem.*, 1969, **32**, 420–424.
30 A. Sluiter, B. Hames, R. Ruiz, C. Scarlata and D. Crocker, *Determination of structural carbohydrates and lignin in biomass*, NREL/TP-510-42618, 2008.
31 W. Zhang, Z. L. Yi, J. F. Huang, F. C. Li, B. Hao, M. Li, S. F. Hong, Y. Z. Lv, W. Sun, A. Ragauskas, F. Hu, J. H. Peng and L. C. Peng, *Bioresour. Technol.*, 2013, **130**, 30–37.
32 Y. Li, P. Liu, J. F. Huang, R. Zhang, Z. Hu, S. Q. Feng, Y. T. Wang, L. Q. Wang, T. Xia and L. C. Peng, *Green Chem.*, 2018, **20**, 2047–2056.
33 R. Zhang, H. Z. Hu, Y. M. Wang, Z. Hu, S. F. Ren, J. Y. Li, B. Y. He, Y. T. Wang, T. Xia, P. Chen, G. S. Xie and L. C. Peng, *J. Exp. Bot.*, 2020, **71**, 2956–2969.
34 M. Madadi, Y. Wang, C. Xu, P. Liu, Y. Wang, T. Xia, Y. Tu, X. Lin, B. Song, X. Yang, W. Zhu, D. Duanmu, S.-W. Tang and L. Peng, *J. Hazard. Mater.*, 2021, **406**, 124727.
35 S. Beck-Candanedo, M. Roman and D. G. Gray, *Biomacromolecules*, 2005, **6**, 1048–1054.
36 Y. Habibi, L. A. Lucia and O. J. Rojas, *Chem. Rev.*, 2010, **110**, 3479–3500.
37 Q. Li, B. Xie, Y. X. Wang, Y. T. Wang, L. C. Peng, Y. Li, B. Li and S. L. Liu, *Food Hydrocolloids*, 2019, **97**, 105214.
38 P. Liu, A. Li, Y. M. Wang, Q. M. Cai, H. Z. Yu, Y. Q. Li, H. Peng, Q. Li, Y. T. Wang, X. Y. Wei, R. Zhang, Y. Y. Tu, T. Xia and L. C. Peng, *Renewable Energy*, 2021, **174**, 799.
39 S.-Y. Ding, Y.-S. Liu, Y. Zeng, M. E. Himmel, J. O. Baker and E. A. Bayer, *Science*, 2012, **338**, 1055–1060.
40 T. Zhang, D. Vavylonis, D. M. Durachko and D. J. Cosgrove, *Nat. Plants*, 2017, **3**, 17056.
41 N. Lin, J. Huang and A. Dufresne, *Nanoscale*, 2012, **4**, 3274–3294.
42 J. Salazar, A. Ghanem, R. H. Muller and J. P. Moschwitzer, *Eur. J. Pharm. Biopharm.*, 2012, **81**, 82–90.
43 M. Lee, M. H. Heo, H. Lee, H. H. Lee, H. Jeong, Y. W. Kim and J. Shin, *Green Chem.*, 2018, **20**, 2596–2610.
44 H. Wang, H. X. Xie, H. S. Du, X. M. Wang, W. Liu, Y. X. Duan, X. Y. Zhang, L. Sun, X. Y. Zhang and C. L. Si, *Carbohydr. Polym.*, 2020, **239**, 116233.
45 Y. X. Zhou, T. Saito, L. Bergstrom and A. Isogai, *Biomacromolecules*, 2018, **19**, 633–639.
46 J. de Aguiar, T. J. Bondancia, P. I. C. Claro, L. H. C. Mattoso, C. S. Farinas and J. M. Marconcini, *ACS Sustainable Chem. Eng.*, 2020, **8**, 2287–2299.
47 K. N. M. Amin, P. K. Annamalai, I. C. Morrow and D. Martin, *RSC Adv.*, 2015, **5**, 57133–57140.
48 H. Hu, R. Zhang, S. Feng, Y. Wang, Y. Wang, C. Fan, Y. Li, Z. Liu, R. Schneider, T. Xia, S.-Y. Ding, S. Persson and L. Peng, *Plant Biotechnol. J.*, 2018, **16**, 976–988.
49 A. N. Fernandes, L. H. Thomas, C. M. Altaner, P. Callow, V. T. Forsyth, D. C. Apperley, C. J. Kennedy and M. C. Jarvis, *Proc. Natl. Acad. Sci. U. S. A.*, 2011, **108**, 1195–1203.
50 M. C. Jarvis, *Carbohydr. Res.*, 2000, **325**, 150–154.
51 Y. Gao, A. S. Lipton, Y. Wittmer, D. T. Murray and J. C. Mortimer, *Nat. Commun.*, 2020, **11**, 6081.
52 K. Herburger, L. Franková, M. Pičmanová, J. W. Loh, M. Valenzuela-Ortega, F. Meulewaeter, A. D. Hudson, C. E. French and S. C. Fry, *Mol. Plant*, 2020, **13**, 1047–1062.